Invited Paper

Fano resonances in the corrugated disk resonator and their applications

Lin Chen [1, 2], Bo Liu [1], and Yiming Zhu [1*, 2]
[1] Shanghai Key Lab of Modern Optical System, University of shanghai for Science and Technology, Shanghai, China
[2] Cooperative Innovation Centre of Terahertz Science, University of Electronic Science Chengdu, China
[*1] Email: ymzhu@usst.edu.cn

(Received December 26, 2017)

Abstract: We have experimentally excited terahertz multipolar Fano resonances in two asymmetrical metal particles: a defective corrugated metallic disk(CMD) structure and a hybrid structure consisted of a C-shaped resonator and a CMD. Furthermore, the Fano resonance modes can also be excited by the interaction between plasmonic waveguide and CMD. Our findings have shed light into the terahertz multipolar Fano resonances in asymmetrical CMD and opened the way to the design of terahertz plasmonic devices.

Keywords: Terahertz, Fano resonances, Corrugated metallic disk

doi:

1. Introduction

Terahertz functional components such as polarizers, modulators and filters, are crucial devices for different terahertz applications [1-10]. Metamaterial is one of particularly interesting components in terahertz region because these metallic microstructured objects derive most of their properties from their ability to support resonances. In the visible and near-infrared regions, the interaction between the wave and the electron plasma is very strong due to large resistivity of metals [11-13]. Then, localized surface plasmons (LSPs) arise around the metallic nanoparticles or nanoshells [13-14] in the visible and near infrared regions. At the very low frequencies of the microwave and terahertz regions, such interaction is very weak because of the high conduction properties of metals at these frequencies [8, 15]. Then, instead of metallic particle, a periodic textured metallic disk structure was proposed to support spoof LSPs [16]. Such spoof LSPs have shown Fano resonances and have been found to be a simpler resonant platform for the microwave and terahertz biosensing by exciting the multipolar resonances of the hybrid metamaterials, exhibiting strong resonance and high Q value [17-19]. In addition, in plasmonic metamaterial,

asymmetric structures are often designed to achieve the excitation of Fano resonance, which comes from the interference dark trapped mode induced by asymmetry of structure with a bright mode [20]. The symmetry breaking in simple structures as an important topic in the field of plasmonics also provides a promising strategy to generate Fano resonance and achieve much stronger electromagnetic field enhancements.

To our knowledge, the experimental verification of multipolar Fano resonances has not been reported in the terahertz range because the excitation of the coaxial antenna source cannot extend its band into the terahertz range in the case of grazing incidence. The work presented in this paper consists of detailed discussions to fully characterize excitation of multipolar resonances in a hybrid structure consisting of a corrugated metallic disk (CMD) coupled with a C-shaped resonator (CSR). The evident transmission dips correspond to resonant modes of high azimuthal order (dipole to decapole modes). This multi-polar spoof LSPs can be seen as dark modes which cannot be directly excited by normal incident wave in symmetric structures. The influence of the inner disk radius r, the filling ratio α, numbers of sectors N, and the gap g on transmission response have also been fully studied. In addition, we find that the higher order Fano resonances (quadrupole to decapole modes) can be generated when the wedge-shaped slice with small angle is cut [19]. Finally, the spoof LSP resonance modes can also be excited by the interaction between plasmonic waveguide and CMD. Fundamental and higher order sharp spoof LSP resonances (from dipole to dodecapole) were observed in the transmission coefficient spectrum. All the results may have potential applications in microchip based sensing and filtering.

2. Spoof localized surface plasmons in corrugated metallic disk coupled to a C- shaped dipole resonator [19]

We investigate the transmission properties of a hybrid spoof LSPs structure consisting of one closed CMD and one C-shaped resonator structure. Figure 1(inset) depicts the schematic diagram of the closed CMD and C-shaped resonator hybrid structure. The angle of the C-shaped resonator $\theta=60^{o}$. The inner radii and width of the CSR are Rc= 160 μm and w=10 μm, respectively. This means the gap between disk and cap is 10 μm. Figure.1 shows that apparent multipolar resonances (marked by C1-C5) can be observed theoretically and most of these resonances (C1-C4) are observed experimentally. The higher resonance (marked by M) rises from the bright LSPs excited by CSR. The electric fields corresponding to dips C1-C5 are shown in Fig.1 (bottom panels). The CSR is resonant as a LSP mode M, while the disk shows multipolar modes, which are in accordance with the spoof LSPs modes of a disk. The resonance M mainly originates from the bright eigenmode of the CSR, while the dark multipole modes from closed CMD cannot be excited to resonate by normally incident wave with transverse polarization. The bottom images in Fig.1 prove that the multipolar modes of the closed disk are excited by the LSP produced at the CSR. In our system, there is only one dark disk and the dark multiple resonances

are induced to be resonant as multipolar modes with spoof LSPs.

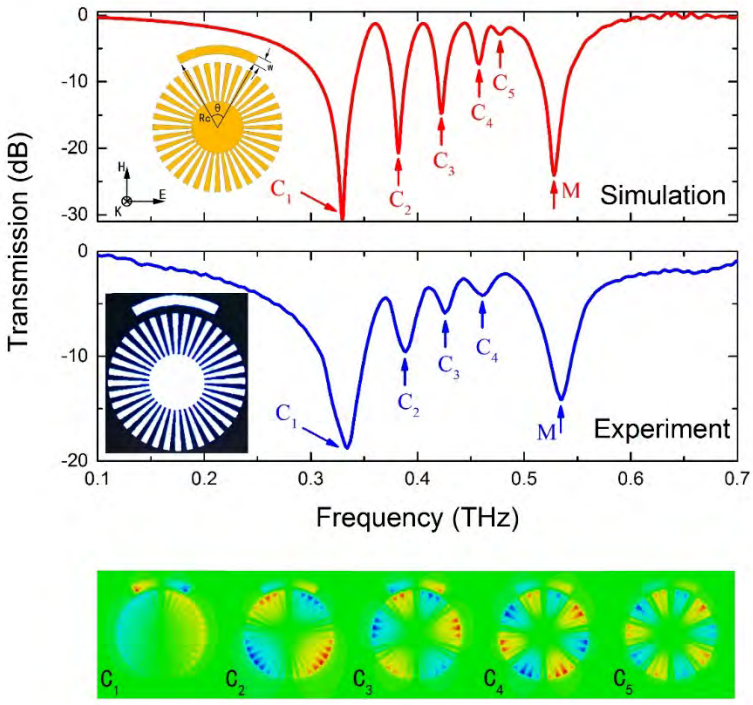

Fig. 1 theoretical and experimental transmission spectra of cap coupled corrugated texturing closed disk, bottom: electric field of multipolar resonances shown as dipole (C1), quadrupole (C2), hexapole (C3), octopole (C4), decapole (C5) mode. The resonance (M) comes from bright LSP mode supported by single CSR structure.

Then, we investigate the effect of parameters influence. Firstly, we analysis the influences of the transmission spectra on the radius of r and R. The simulated dispersion curves of the corresponding corrugated metallic strips are shown in Fig.2 with R = 150 μm, N = 36, d = 2πR/N, a = 0.4d and different inner radius r. The transmission spectra with different r are plotted in Fig.3. It is clearly observed that the blueshift property of LSP resonance frequencies with inner radius r plotted in Fig.3 is actually consistent with the dispersion relations shown in Fig.2. When the inner radius r increases from 15 μm to 90 μm, the asymptote frequency of dispersion curves increases from 0.35 *THz* to 0.752 *THz* (Fig.2), and blueshifts of the spoof LSPs frequencies are observed (Fig.3). We note that the highest order resonances of spoof LSPs (in Fig.3) approximate the corresponding asymptote frequencies (in Fig.2). As spoof LSP resonance frequency is close to asymptote frequency, the propagation of terahertz wave is slower and its field is more tightly confined to the corrugated metal disk, leading to weakening of the intensity of the corresponding spoof LSPs, as shown in Fig. 3. In addition, for r=75 μm and 90 μm, the asymptote frequencies are 0.612 *THz* and 0.752 *THz*, respectively, which overlap the resonance frequency of CSR (in Fig.3). Here some higher order spoof LSP modes exhibit mode splitting effect, which may be due to the interaction between spoof LSP mode and CSR mode. As a consequence, the inner radius r has a significant impact on the spoof LSP resonance frequency.

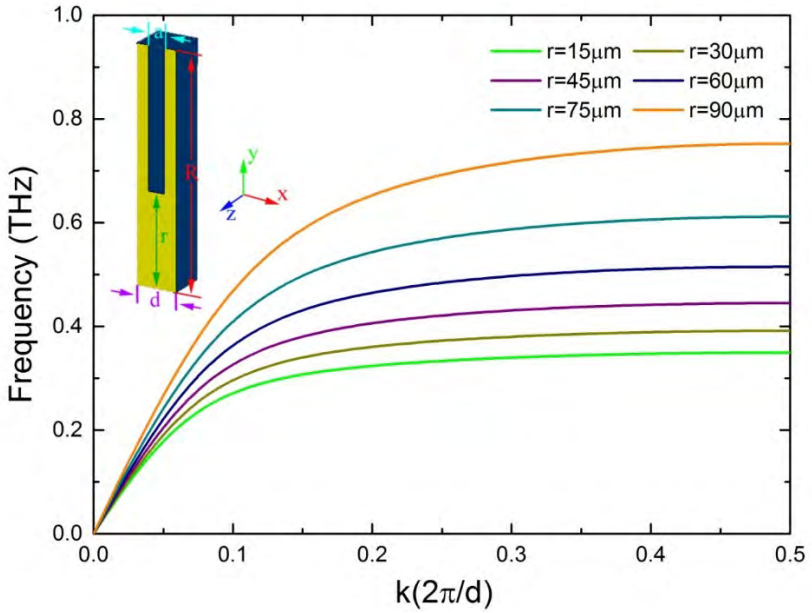

Fig. 2 Simulated dispersion curves of spoof LSPs for one periodic corrugated strips (see in set) with $R = 150\ \mu m$, $N = 36$, $d = 2\pi R/N$, $a = 0.4d$, and different lengths of r.

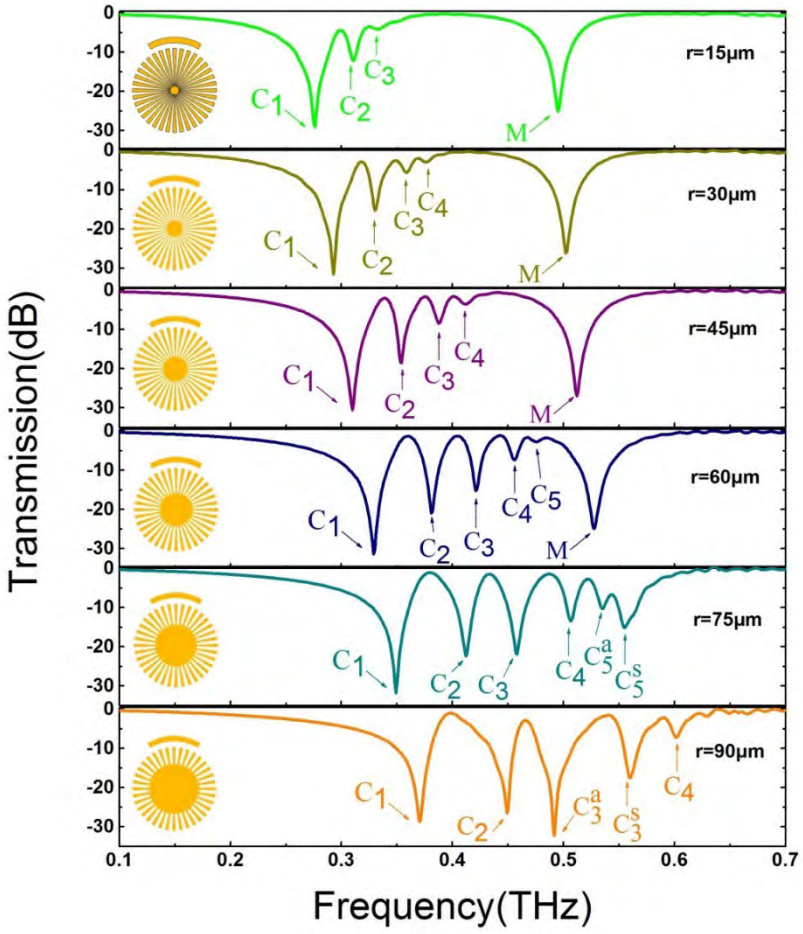

Fig. 3 Transmission spectra with respect to various disk inner radius r.

Next, we discuss the influence of the ratio α and N. Fig.4 illustrates that the ratio α affects slightly the asymptote frequencies of the spoof surface plasmon polaritons(SPPs), yielding a tiny redshift of the LSP resonances with increasing filling ratio. And the resonance frequencies of the spoof LSPs are independent of the numbers of sectors N (in Fig.5). This observation can be understood through the Equation of asymptote frequency of the spoof surface plasmons, which can be roughly written as $\omega_a = \pi c/(2hng)$, where c is the light speed, ng is the refractive index of the media filled in the grooves (in this work ng =1), and h represents the depth of the groove, which is R− r. Thus, the asymptote frequency and related spoof LSP resonance frequency are nearly independent of the filling ratio α and numbers of sectors N.

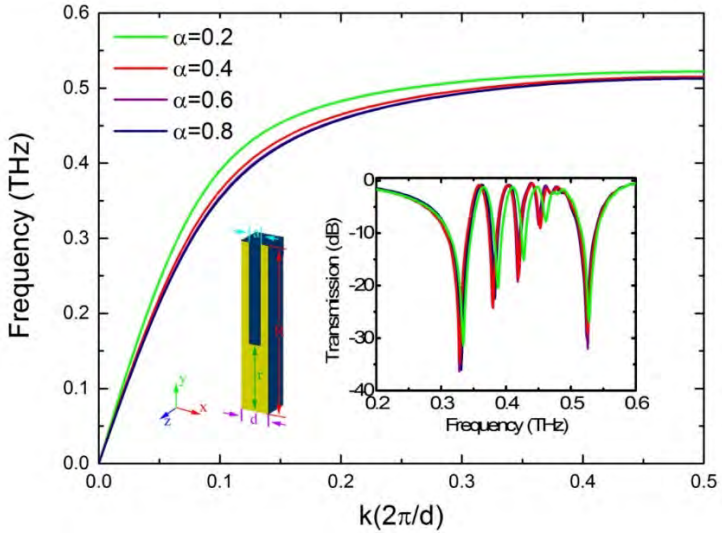

Fig. 4 Dispersion curves for the corrugated metallic disk with different α (a/d). (inset) Transmission spectra for corrugated metallic disk coupled to a C shaped dipole resonator with different α. The other parameters are R = 150 μm, N = 36, $d = 2\pi R/N$, and r=60 μm.

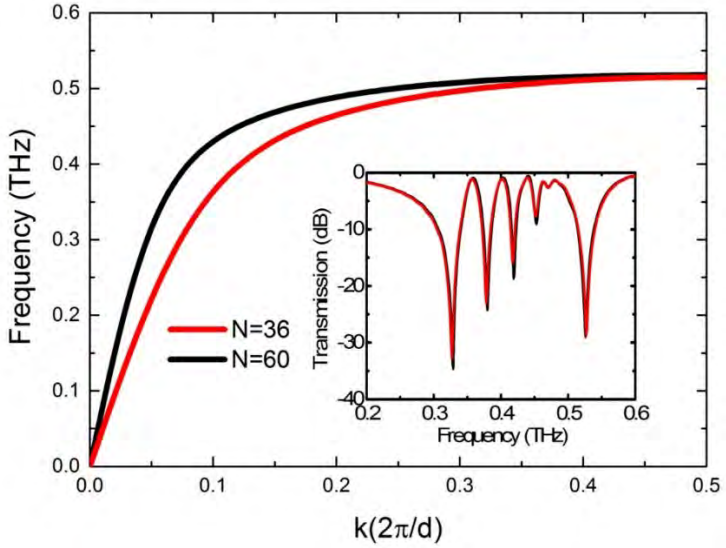

Fig. 5 Dispersion curves for the corrugated metallic disk with different N. (inset) Transmission spectra for corrugated metallic disk coupled to a C-shaped dipole resonator with N=36 and 60. The other parameters are R = 150 μm, $\alpha = a/d$ = 0.4, $d = 2\pi R/N$, and r = 60 μm.

The highest order resonances of spoof LSPs approximate the corresponding asymptote frequencies of SPP (or LSP). Then, theoretically multipolar resonance can be excited as its resonance frequency is lower than asymptote frequency in dispersion curve. However, the resonance frequency of CSR plays an important role to excite multipolar resonance. If the resonance frequency of CSR is far away from the asymptote frequency of structure, high orders resonances can hardly be efficiently excited. While the resonance frequency of CSR overlaps asymptote frequency of structure, there is the interaction between spoof LSP modes and CSR mode. According to Fig 2, the highest order dipole is decapolar. Because the intensity of the highest order spoof LSPs is weaker as spoof LSP resonance frequency is close to asymptote frequency, such highest order resonance can hardly be observed due to the additional loss from polyimide loss and fabrication error.

3. Fano resonances induced by the asymmetry due to defect in the corrugated disk resonator [21]

In Fig.6, we schematically illustrate the geometry of meta-atom with defective angle θ, which are composed of outer disk radius R = 150 μm and inner metallic disk of radius r = 60 μm surrounded by N = 36 periodically radical metallic grooves with the periodicity d = 2πR/N. The parameterα=a/d=0.4 is the air-filled ratio in the single periodic structure (a: groove width) and thickness of the metallic film (aluminum, σ_{Al}=3.56 × 107 S·m^{-1}) disk t=200 nm. The metallic disk is based on a 22 μm-thick mylar substrate. The period of the unit cell is 360 μm. Numerical simulations were performed using CST Microwave Studio to obtain the transmission response of the defective (θ=14º) CMD structures, with the E-field polarized perpendicular to the defective wedge-shaped slice, as shown in Fig.6(b). We fabricated the defective CMD using conventional lithography (the microscopic image of the structure is shown in Fig.6(c)). The meta-atom array chip has a size of 10×10 mm^2. A blank mylar identical to the one on which the defective CMDs were fabricated was used as a reference.

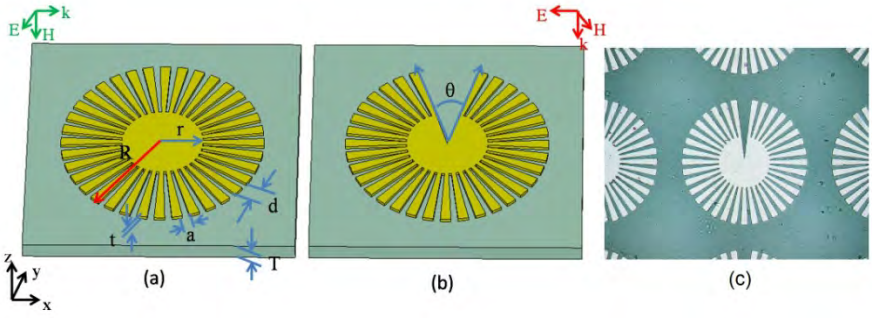

Fig. 6 Schematics of the planar CMD (a) and defective CMD (b) meta-atom. r = 60 μm, R = 150 μm, N=36, d = 2πR / N, a = 0.4d, θ = 14º. (c) Microscopic image.

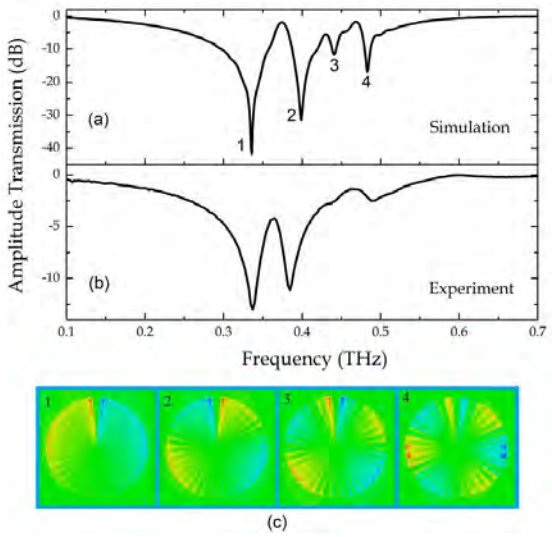

Fig. 7 (a) Theoretical and (b)experimental transmission spectra of defective CMD with θ=14°.(c) the electric field at resonant frequencies with defective angle θ=14°. Modes 1, 2, 3 and 4 correspond to dipole, quadrapolar, hexapolar and octopolar modes, respectively.

The amplitude transmission spectra through the samples were measured using a confocal photo-conductive-based 8f terahertz time-domain spectroscopy system [22]. The simulated, experimental and electric field distributions at the resonance dips (1, 0.312 *THz*; 2, 0.376 *THz*; 3, 0.415 *THz*; 4 0.451 *THz*) are shown in Fig.7, where these four resonant modes correspond to di-(1), quadru-(2), hexa-(3) and decapole(4) resonance modes, respectively. As shown in Fig.7(c), The electric-field lines of both dipolar slice mode and dipolar spoof LSP mode propagate from positive charges and arrive at negative charges. Somode 1 (dipole) corresponds to the hybridized bright mode, where the dipolar slice mode and the dipolar spoof LSP mode oscillate in phase, resulting in an increased superradiative damping. Mode2 (quadrapolar mode) corresponds to the quadrupolar Fano resonance resulting from the coupling of the dipolar slice mode and the quadrupolar spoof LSPs. It should be note that the bright wedge defect dipole mode strongly interacts with the nearby polars of dipole and quadrapole, which have covered large area with several numbers of sectors. So nearly perfect dipole and quadrupole patterns can be found in Fig.7(c). The resonant behaviors for modes 3 and 4 indicate that though two Fano modes result from the interaction between the dipolar slice mode and the multipolar spoof LSP modes (hexapolar and octopolar modes), the wedge defect deeply affects the approaching polars of hexa/octopolar modes, leading to the slight distortions of electric distributions compared with regular hexapolar and octopolar modes, as shown inFig.7(c). As a result, the hexa/octopolar modes can't be fully excited and the electric field distributions don't show the standard hexa/octopolar patterns due to the asymmetry of single defect structure.

It is interesting to reveal how the dark Fano resonances are affected by varying the angle of defect θ. Fig.8shows the transmission with the increase of angle of defect from 14° to 24°. We can see that firstly, the resonance 3(4) becomes weaker with the increase of angle of defect because the polar of resonance 3(4) near defective slice edge becomes small and the distortion of

electric field of hexa-(octo-) polar Fano modes has generally deteriorated. In contrast, the hybridized dipole mode and the quadrupolar Fano resonance are observed more clearly.

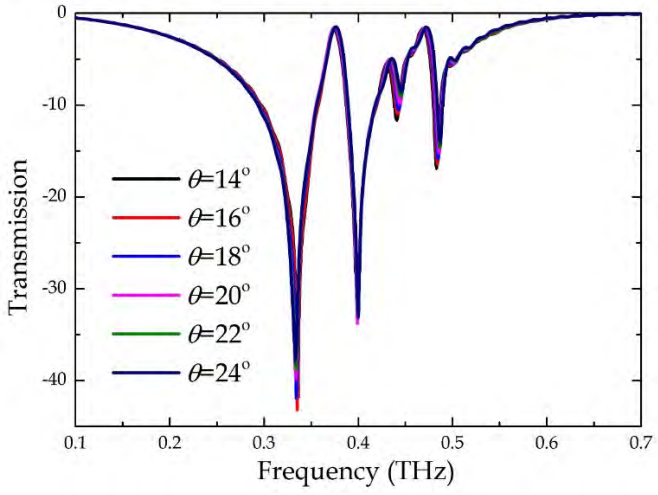

Fig. 8 transmission spectra at angles from 14° to 24°

It is interesting to see that the quadrupolar peak show high Q feature in Fig.7(b), which may enable ultrasensitive sensing. we choose the sharp quadrupolar peak and the higher dip (compared with two dips) on the resonance curve as two extreme points and then note the full-width at half-maximum(FWHM=Δf=f_2-f_1) bandwidth. Taking the ratio of the resonance frequency at peak, and the FWHM, i.e., $f_0/\Delta f$, we obtain the value for the Q-factor. The key parameters of Q-factor calculation of single defect structure can be listed as follows:

Tab. 1 the key parameters about Q-factor calculation

θ	f_0	f_1	f_2	Δf	Q
6	0.387	0.3825	0.3916	0.0091	42.52747
8	0.383	0.3779	0.38784	0.00994	38.53119
10	0.38	0.3748	0.3853	0.0105	36.19048
12	0.377	0.3718	0.38285	0.01105	34.11765
14	0.374	0.3684	0.3799	0.0115	32.52174
16	0.375	0.3689	0.3803	0.0114	32.89474
18	0.375	0.3689	0.3803	0.0114	32.89474
20	0.375	0.36905	0.3807	0.01165	32.18884
22	0.376	0.37	0.3815	0.0115	32.69565
24	0.376	0.3703	0.38184	0.01154	32.58232

As can be seen, the quadrupolar transparency peak shows high Q-value and high figure of merit (FoM)features.

4. Sensing chip consist of a plasmonic waveguide with a corrugated disk resonator[23]

The bilateral symmetric corrugated metallic structures are illustrated in Fig.9(a). It illustrates a schematic configuration of the high-efficiency coplanar waveguide (CPW) and a thin corrugated disk resonator (CDR). The structure includes three parts: I. an energy transition section, II. a mode conversion and momentum matching section, III. plasmonic waveguide with a CDR. The plasmonic waveguide port 1 and 2 can be used as signal input and output port, respectively. Fig.9(b)、(c) and (d) show details of each part, respectively, marked as part I, II and III. The spacing between the plasmonic waveguide and CDR is g. The width and periodicity of the grooves are denoted as a=0.5d, $p=\frac{2\pi R}{N}$, where N=20 is the total number of grooves. The outer radius of the corrugated disk and the number of grooves are chosen to satisfy $d \ll \lambda$. The height of waveguide is h. The dimensions mentioned above are R=1200 μm, r=600 μm, h_1=500 μm, h_2=450 μm, and p=380μm.The numerical simulation of the designed sensor chip was carried out by using commercial software, CST Microwave Studio. The boundary conditions of x, y, z are open. To simulate the wave propagate in free space. Gold layer was modeled as lossy metal and behave almost like perfect conductor compared to visible region [11], and the quartz substrate is taken as a lossy material with dielectric loss tangent of tan(δ)= 0.0004. The surface metal layer is 0.5 μm-thick gold，and is fabricated by conventional lithography. In order to reduce the loss of this part, we can choose the excellent performance medium such as gallium arsenide, sapphire, quartz as the substrate material. In this paper, quartz is used as the substrate, which is 200 μm-thick.

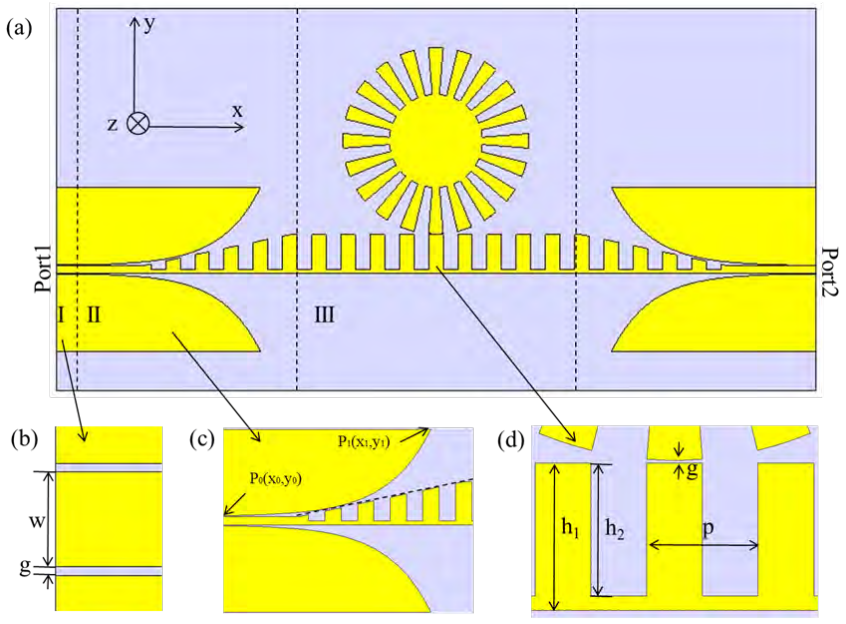

Fig. 9(a) The top view of high-Q plasmonic waveguide with corrugated disk resonator system, which is divided into three comparatively independent regions (I, II and III). (b) Part I: the CPW region. (c) Part II: the convertor, which converts QTEM mode to spoof mode. (d) Part III: plasmonic waveguide with corrugated disk resonator.

The simulated transmission coefficient (dB) is shown in Fig.10(a), the red curve shows the plasmonic waveguide with CDR and the black curve shows the feature of the broadband transmission when without corrugated disk resonator. With the corrugated disk, the six main dips are generated by coupling resonance between plasmonic waveguide and corrugated disk. Each of dip corresponds to a different mode [24], which is marked in Figure.10(a) (red curve). Figure.10(b)-(g) illustrate the electric field (Ez) on an x-y plane which is 0.1 *mm* above the metal film. Dips 1-6 in Figure.10(a) correspond to resonance mode in Figure.10(b)-(g). Dips 3-5 in the simulation band are quite obvious and have high-Q factors. These three dips Q factors are 44.6, 268.3 and 215.8, respectively. It can serve as good features for biosensor. In the experiment, we mainly focus on these three high-Q dips (3-5).

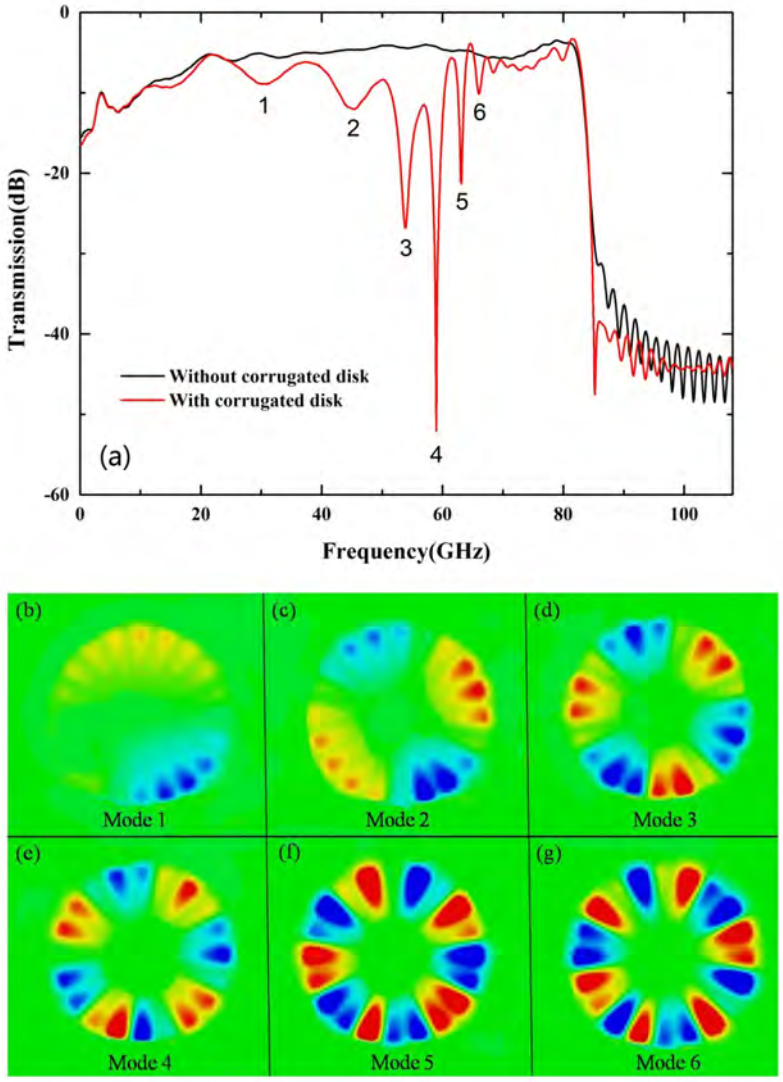

Fig. 10(a) The transmission coefficients S21 of the biosensor system, in which the black line stands for the plasmonic waveguide without corrugated disk, and the red line stands for the spoof SPP waveguide with corrugated disk, (b)-(g) the electric field (E_z) on an x-y plane which is 0.1mm above the metal film.

Next, we analyze the resonance frequencies of these dips (1-6). The phase change around the corrugated disk is calculated as [25]:

$$\Delta\varphi = \frac{2\pi}{\lambda} n_e 2\pi R \qquad (1)$$

where β is the propagation constant. The coherence condition must be met for constructive (destructive) interference when the output wave is enhanced (closed); in other words, the circumference of the resonator must be an even (odd) number of wavelengths or frequencies of the resonant modes for constructive (destructive) interference, that is

$$\Delta\varphi = 2m\pi \ (\Delta\varphi = (2m+1)\pi) \qquad (2)$$

In order to investigate the position of resonant dips, we focus on the destructive interference. Substituting Eq. (2) into Eq. (1), we get

$$(2m+1)\pi = \beta \cdot 2\pi R \qquad (3)$$

If we define $k = \frac{\beta}{2\pi/p}$ is the normalized wavenumber ($p = \frac{2\pi R}{N}$ is the periodic constant of CDR), Eq. (3) can be rewritten as

$$k\left(\frac{2\pi}{p}\right) = \frac{\beta}{2\pi/p} = \frac{2m+1}{2R} \cdot \frac{p}{2\pi} = \frac{2m+1}{2N} \qquad (4)$$

When the disk at the closed state, there is a relative relationship between k and m. And it is shown in the following Table 2. The close state frequencies from the dip 3 to 5 on the S21 parameter and the frequencies from the corrugated disk dispersion curve are in an agreement.

Tab. 2 Theoretical and numerical resonance frequencies of different modes

m	k ($2\pi/p$)	Frequency(GHz) from the dispersion curve	Frequency(GHz) from the S21 parameter
3	0.175	53.8	53.8
4	0.225	60.1	59.0
5	0.275	64.2	64.6

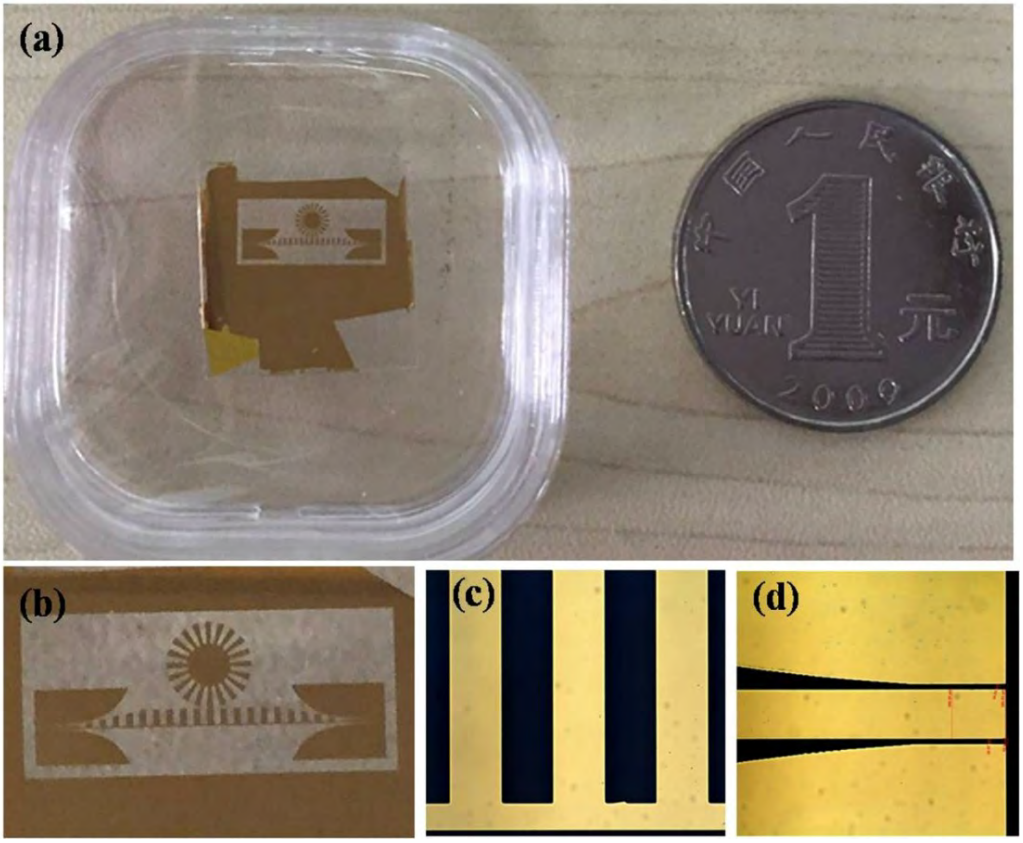

Fig. 11 (a)-(b) The photograph of the sample in a membrane box; (c)-(d) Detailed picture under a microscope

The biosensor system sample is shown in Fig.11 (a). In the experiment, the total size of quartz substrate is 15 *mm*×15 *mm* (Fig.11 (b)). The structure (CPW, waveguide and CDR) is fabricated by conventional lithography. Fig.11(c)-(d) are photographs of plasmonic waveguide and CPW. The transmission coefficient S21 was measured by Agilent N5245A vector network analyzer (the frequency band is 50-75 *GHz*, which covers mode 3-5). The probe pins are placed at port 1 and 2, respectively. The simulation and experiment results (without detect material) are shown in Fig.12 (black curve). The modes 3-5 were appeared clearly in the transmission spectra. The experimental (simulated) resonance frequences are 53.7 *GHz* (53.9 *GHz*), 59.2 *GHz* (59.0 *GHz*) and 63.3 *GHz* (63.2 *GHz*), respectively. And the experimental (simulated) transmission coefficient (dB) can reach -28.9 *dB* (-28.6 *dB*), -39.8 *dB* (-52.1 *dB*) and -18.1 *dB* (-21.3 *dB*), respectively. In experiment, the Q-value of octupolar mode has been observed as high as 268.3, which is suitable for sensing application. Experimental result shows a good agreement with simulation. The slight difference between simulation and experiment is caused by fabrication and measurement tolerances.

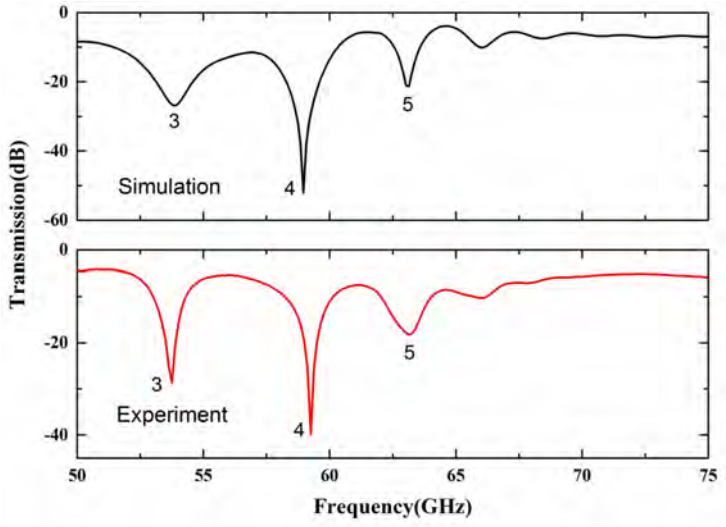

Fig. 12 Simulated and measured transmission coefficients S_{21} with CDR

The corrugated disk resonances are sensitive to the change of surrounding materials. If the permittivity ε is changed within the corrugated disk grooves, all the resonance dips will shift. For the corrugated disk grooves filling different refractive index materials, the resonance will be changed significantly. The permittivity of the inner environment increases, which makes the resonance frequency red-shift, and can be used ad spectral signatures to identify the unknown materials [26]. From the simulation results, we change the permittivity ε from 1.02 to 1.1. In Fig.13, when ε increases, the resonance dips red-shift moves to the lower frequencies.

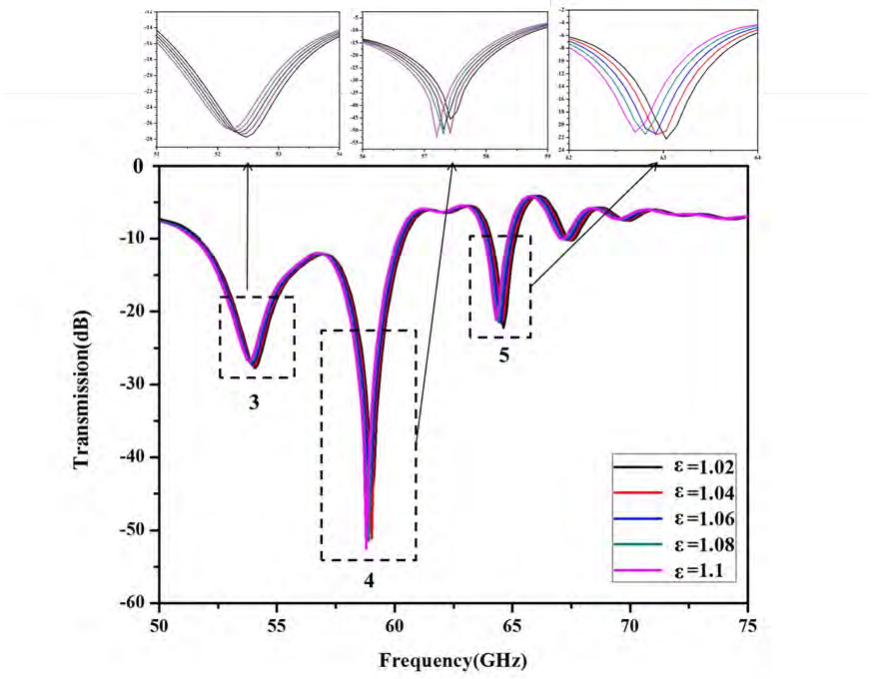

Fig. 13 Red-shift of the resonance dips

The corrugated disk is an important part of the biological sensor system,/. We can fill different detected materials in the groove of the corrugated disk. Since both solid and liquid can be measured, we choose different liquids in the experiment. We use cotton swab dipped in liquid, then cover the groove of liquid. When a liquid is replaced, the sensor sample is placed in the acetone and then deionized water. The low power ultrasonic cleaning machine is used for cleaning. The fillers as we used in experiments to filling the corrugated disk grooves are ethanol, deionized water and olive oil. From the measured results, we observe that the resonant frequencies have significant shifts by covering different detected materials. From Fig.14, by filling different transparent liquids, unknown transparent liquids can be identified by measuring resonance red-shift resulting from the refractive index changes of the fillers. We have found that in addition to the red-shift, these dips' transmission coefficients (dB) are also different. This may be due to the different influence of the electric field around the corrugated disk with different liquid concentration. In Shen et al. [18], they obtain a 0.45 *GHz* shift in the hexapole resonance and 0.55 *GHz* shift in the octopole resonance for a 61% change in index (from n=1 to n=1.61). In our simulation, we obtain a 0.22 *GHz* shift in the hexapole and octopole resonance (from ε=1.02 to ε=1.1). Our sensor-ship is compact and easy integrated. Its coupling way is through CPW converts the guide waves to spoof SPPs with high efficiency in broadband. It can be applied in the detection of micro materials in THz band.

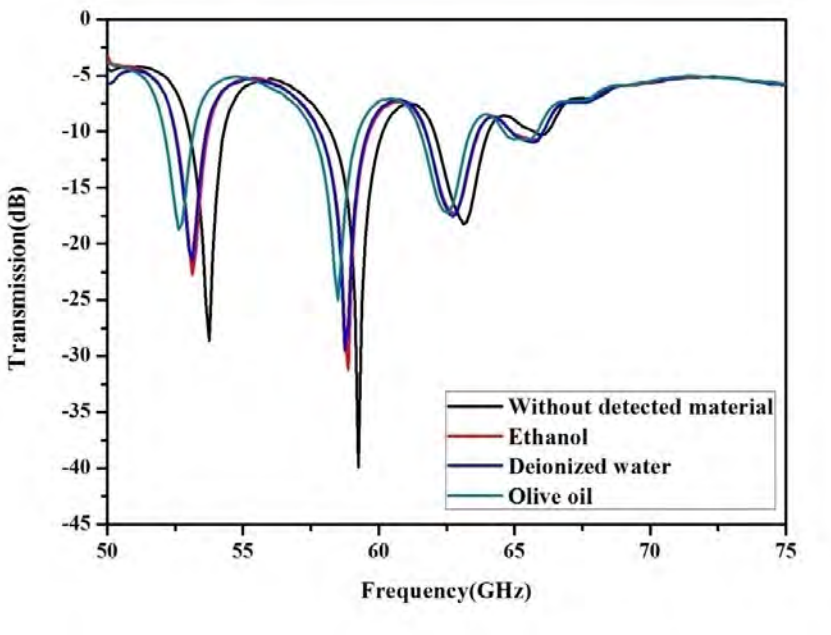

Fig. 14 Detection of different liquid in the corrugated disk groove

5. Conclusion

We theoretically and experimentally introduce the excitation of terahertz multipolar spoof LSP resonances in the transmission spectra at normal incidence in a hybrid structure consisting of a

CMD coupled with a CSR. Then, we propose novel planar metaatom structures supporting multiple Fano resonances. The unit cell consists of a defective CMD structure. Numerical and experimental results reveal that multiple Fano resonances could be excited at terahertz frequencies when the symmetry of CMD is broken by introducing a small angle of defect. Such multiple Fano resonances result from mutual coupling between bright dipolar mode evoked by the edge of the wedge-shaped slice and dark multipolar spoof LSP modes. Furthermore, the effects of the defect angle on Q-factors and intensities of the quadrupole peak mode are investigated. Large FoMof 16 is achieved. Finally, we have designed and fabricated a sensing chip consist of a CPW and plasmonic waveguide with a corrugated disk resonator. We show that the spoof SPP resonance modes are excited by the interaction between plasmonic waveguide and corrugated disk resonator. There are six resonance dips, and three dips are obvious sharply. We distinguish different materials to detect sensitivity of sensing chip by experiment.

Reference

[1] Piesiewicz, R., Ostmann, T. K., Krumbholz, N., et al.. “Short-range ultrabroadband terahertz communications: Concepts and perspectives”. *IEEE Antennas Propag. Mag*., 49, 24-39 (2007).

[2] Mendis, R., Nag, A., Chen, F., et al.. “A tunable universal terahertz filter using artificial dielectrics based on parallel-plate waveguides”. *Appl. Phys.Lett.*, 97, 131106 (2010).

[3] Chen, L., Truong, K. V., Cheng, Z. X., et al.. “Characterization of photonic bands in metal photonic crystal slabs”. *Opt. Commun.*,333, 232–236 (2014).

[4] Chen, L., Gao, C. M., Xu, J. M., et al.. “Observation of electromagnetically induced transparency-like transmission in terahertz asymmetric waveguide-cavities systems”. *Opt. Lett.*, 38, 1379-1381 (2013).

[5] Chen, L., Xu, J. M., Gao, C. M., et al.. “Manipulating terahertz electromagnetic induced transparency through parallel plate waveguide cavities”. *Appl. Phys. Lett.*,103, 251105 (2013).

[6] Chen, L., Cheng, Z., Xu, J., et al.. “Controllable multiband terahertz notch filter based on a parallel plate waveguide with a single deep groove”. *Opt. Lett.*, 39, 4541-4544 (2014).

[7] Xu, J. M., Chen, L., Zang, X. F., et al.. “Triple-channel terahertz filter based on mode coupling of cavities resonance system”. *Appl. Phys. Lett.*,103, 161116 (2013).

[8] Chen, L., Zhu, Y. M., Zang, X. F., et al.. “Mode splitting transmission effect of surface wave excitation through a metal hole array”. *Light Sci. Appl.*, 2, e60 (2013).

[9] Singh, R., Rockstuhl, C., Lederer, F., et al.. “Coupling between a dark and a bright eigenmode in a terahertz metamaterial”. *Phys. Rev. B*, 79, 085111(2009).

[10] Qu, D., Grischkowsky, D., and Zhang, W. “Terahertz transmission properties of thin, subwavelength metallic

hole arrays". *Opt. Lett.*, 29, 896-898 (2004).

[11] Chen, L., Cao, Z. Q., Ou, F., et al.. "Observation of large positive and negative lateral shifts of a reflected beam from symmetrical metal-cladding waveguides". *Opt. Lett.*, 32, 1432-1434 (2007).

[12] Chen, L. Cheng, Z. X. and Zhu, Y. M. "Influence of slanted guiding layer on reflection curve and sensitivity for air-gap displacement sensor". *J. Mod. Opt.*, 61(11), 938-942 (2014).

[13] Chen, L., Liu, X. B., Cao Z. Q. et al.. "Mechanism of giant Goos–Hänchen effect enhanced by long-range surface plasmon excitation". *J. Opt*., 13, 035002 (2011).

[14] A. Evlyukhin, C. Reinhardt, and B. Chichkov. "Multipole light scattering by nonspherical nanoparticles in the discrete dipole approximation". *Phys. Rev. B*, 84, 235429 (2011).

[15] J. B. Pendry, L. Martín-Moreno, and F. J. Garcia-Vidal. "Mimicking surface plasmons with structured surfaces". *Science*, 305, 847–848(2004).

[16] A. Pors, E. Moreno, L. Martin-Moreno, et al.. "Localized Spoof Plasmons Arise while Texturing ClosedSurfaces". *Phys. Rev. Lett*., 108, 223905 (2012).

[17] Lu, X., Han, J., and Zhang, W. "Localized plasmonic properties of subwavelength geometries resonating at terahertz frequencies". *IEEE J. Sel. Top. Quant.*, 17, 119-129 (2011).

[18] Shen, X., and Cui, T. J. "Ultrathin plasmonic metamaterial for spoof localized surface plasmons". *Laser Photon. Rev.*, 8, 137–145 (2014).

[19] Chen, L., Wei, Y. M., Zang, X. F., et al.. "Excitation of dark multipolar plasmonic resonances at terahertz frequencies". *Sci. Rep.*, 6, 22027 (2016).

[20] L. Cong, M. Manjappa, N. Xu, et al.. "Fano Resonances in Terahertz Metasurfaces: A Figure of Merit Optimization". *Adv Optical Mater.*, 3, 1537-1543 (2015).

[21]Chen L, Xu N, Singh L, et al. "Defect- Induced Fano Resonances in Corrugated Plasmonic Metamaterials". *Adv Optical Mater.*, 5(8),1600960(2017).

[22] D. Grischkowsky, S. Keiding, M. Exter, Ch. Fattinger, *J. Opt. Soc. Am. B*, 7, 2006(1990).

[23] WangDanni, et al. "Spoof Localized Surface Plasmons Excited by Plasmonic Waveguide Chip with Corrugated Disk Resonator". *Plasmonics*, 12,947-952(2017).

[24] Ali K. Horestani, WithawatWithayachumnankul, Abdallah Chahadih, et al.. "Metamaterial-Inspired Bandpass Filters for TerahertzSurface Waves on Goubau Lines". *IEEE Trans. Terahertz Sci. Technol.*, 3 (2013).

[25] G. Goubau. "On the excitation of surface waves". *Proc. IRE*, 40, 865-868 (1952).

[26] Chen Z, Mohsen R, Gong Y, et al.. "Realization of variable three-dimensional terahertz metamaterial tubes for passive resonance tenability". *Adv Mater.*, 24, 143–147(2012).